HHS Public Access

Author manuscript

Magn Reson Med. Author manuscript; available in PMC 2017 June 01.

Published in final edited form as:

Magn Reson Med. 2016 June ; 75(6): 2573–2578. doi:10.1002/mrm.25850.

Sensitivity Enhancement of an Inductively Coupled Local Detector Using a HEMT-based Current Amplifier

Chunqi Qian[1,2], **Qi Duan**[1], **Steve Dodd**[1], **Alan Koretsky**[1], and **Joe Murphy-Boesch**[1]

[1]Laboratory of Functional and Molecular Imaging, National Institute of Neurological Disorders and Stroke, National Institutes of Health, Bethesda, Maryland, USA

[2]Department of Radiology, Michigan State University, East Lansing, MI, USA

Abstract

Purpose—To improve the signal transmission efficiency and sensitivity of a local detection coil that is weakly inductively coupled to a larger receive coil.

Methods—The resonant detection coil is connected in parallel with the gate of a HEMT transistor without impedance matching. When the drain of the transistor is capacitively shunted to ground, current amplification occurs in the resonator by feedback that transforms a capacitive impedance on the transistor's source to a negative resistance on its gate.

Results—High resolution images were obtained from a mouse brain using a small, 11 mm diameter surface coil that was inductively coupled to a commercial, phased array chest coil. Although the power consumption of the amplifier was only 88 μW, 14 dB gain was obtained with excellent noise performance.

Conclusion—An integrated current amplifier based on a High Electron Mobility Transistor (HEMT) can enhance the sensitivity of inductively coupled local detectors when weakly coupled. This amplifier enables efficient signal transmission between customized user coils and commercial clinical coils, without the need for a specialized signal interface.

Introduction

The sensitivity of magnetic resonance imaging and spectroscopy is critically dependent on the performance of the coil and preamplifier. In the standard configuration, the sample coil L_0 is tuned by a parallel capacitor C_0 and impedance matched to 50 Ω (1). Alternatively, NMR signals from an isolated coil can be transmitted to an external coil through mutual inductive coupling (2). To improve local sensitivity of the isolated resonator, the sample coil can be miniaturized and placed in very close proximity to the object being imaged (3). When a passive *LC* resonator is used deep inside the body as a wireless, implantable detector (2), this mutual coupling may be too weak to enable efficient signal transmission. To compensate for transmission loss in weakly coupled conditions, it has been demonstrated that a parametric amplifier can be integrated into an *LC* resonator for *in situ*, wireless

Correspondence: Chunqi Qian, 10 Center Dr Rm 1D48, National Institute of Health, Bethesda, MD, 20892, Tel: +1 (301) 435-2146; Fax: +1 (301) 480-2558, qianc2@ninds.nih.gov.

amplification of MR signals (4,5). Parametric amplifier is a multi-frequency resonator that relies on nonlinear capacitance to transfer energy from the high energy pumping signal to the low energy MR signal (6,7). Although the parametric resonator has the great advantage that it can operate wirelessly, noise is introduced during frequency mixing, limiting the amplifier's noise figure to 3 dB (8).

Here, we utilize positive feedback from a transistor connected in parallel with the LC resonator to develop an equivalent, negative parallel resistance for *in situ* signal amplification. Unlike standard transistor-based amplifiers, where the input voltage on the gate is converted to a modulated current on the drain, the negative resistance amplifier creates feedback current that adds in phase with the current circulating in the LC circuit to produce a net current gain (9). The drain of the transistor is grounded with a large value capacitor and a small capacitor is placed between the source and ground. The high impedance of the source capacitor creates voltage feedback through the gate capacitance to obtain a negative resistance R_{neg} across the LC circuit. The parallel resistance R_{LC} of the LC circuit is increased to $R_{LC}|R_{neg}|/(|R_{neg}|- R_{LC})$, and the effective quality factor of the resonator is increased to

$$Q_{\text{eff}}=Q_{LC}|R_{\text{neg}}|/(|R_{\text{neg}}| - R_{LC}). \quad [1]$$

The current gain in the LC circuit is Q_{eff}/Q_{LC}, so the weak voltage drive from the NMR resonance induces a much larger current in the LC circuit than in the passive coil. The amplifier uses a High Electron Mobility Transistor (HEMT), and because current amplification occurs without the need for frequency mixing, the amplifier has good noise performance. Although the current version of amplifier requires a bias voltage, it operates with a very low bias current and can be powered for very long intervals (weeks) with a non-magnetic battery, enabling application as a wireless implantable device. Here, it is connected to a 11 mm diameter coil optimized using a saline phantom to simulate tissue loading. The circuit was tested for SNR on a clinical 3T system using a commercial phased array as the external receiver. The coil and amplifier coupled to the clinical coil were then evaluated over a range of distances to determine the effect upon SNR. The circuit was then used to image a mouse brain, with the animal and local coil situated beneath the clinical coil.

Methods

The integrated amplifier is shown schematically in Fig. 1a, with the HEMT transistor (Agilent ATF-34143) placed in parallel with the LC resonator. The sample coil, shown in Fig. 1b, was an 11 mm diameter, single turn inductor (L_0=24 nH) printed on a G10 substrate. The tuning capacitor C_0 (62 pF) was chosen to resonate the coil slightly above the Larmor frequency at 123.24 MHz. Precise frequency adjustment was accomplished with the trim capacitor C_t (Johanson 9702-2) connected across C_0. A crossed diode pair (BAT15-04W, Infineon Technologies, Germany) connected across C_0 was used to passively detune the LC resonator during RF excitation. The drain of the transistor was RF grounded with a 10 nF capacitor. The circuit was powered at the transistor drain with an adjustable voltage (V_1). The gate capacitance C_g was increased by 1.5 pF to increase amplifier gain. Positive feedback from the transistor creates negative resistance between the gate terminal and

ground. The magnitude of this negative resistance is dependent upon the gate capacitance C_g, the source capacitance C_s and the transconductance g_m. C_g between the transistor gate and source terminals has no easy access for dynamic control. Therefore, the source capacitance C_s was replaced with a varactor (BBY51-02W, Infineon Technologies, Germany) whose capacitance was varied with a second bias voltage V_2 applied on the cathode via a large (100 kΩ) resistor.

To understand the current feedback mechanism, a small signal model of the transistor (8) was used (Fig. 1c). The RF drain-source current is given by $I_{ds}=g_m V_{gs}$, and the gate current by $I_{gs}=j\omega C_g V_{gs}$. The total RF current through the impedance Z_s is the sum of the two, $I_{ds}+I_{gs}$, and the admittance between the gate and ground can be expressed as,

$$Y_g=\frac{I_{gs}}{V_{gs}+V_s}=\frac{I_{gs}}{I_{gs}/j\omega C_g+(I_{gs}+I_{ds})Z_s}=\frac{j\omega C_g}{1+(j\omega C_g+g_m)Z_s}. \quad [2]$$

When the source impedance Z_s is capacitive, i.e. $Z_s = 1/j\omega C_s$, the admittance becomes

$$Y_g=\frac{-\omega^2 C_s C_g}{j\omega C_g+j\omega C_s+g_m}=\frac{-\omega^2 C_s C_g g_m+j\omega^3 C_s C_g(C_s+C_g)}{g_m^2+\omega^2(C_s+C_g)^2}. \quad [3]$$

An equivalent representation of the real and imaginary components is illustrated in Fig. 1d. The real part of Y_g is negative, and it can be converted into a negative resistance,

$$-R_{\text{neg}}=\frac{g_m}{\omega^2 C_s C_g}+\frac{(C_s+C_g)^2}{C_s C_g g_m}. \quad [4]$$

Eq. [4] can be minimized with respect to any of the variables, g_m, C_s, or C_g. However, with g_m and C_g fixed, Eq. [4] is minimized when $C_s^2 = C_g^2 + g_m^2/\omega^2$. Using this relation to eliminate C_s, $|R_{neg}|$ has a minimum at

$$-R_{\text{neg}}=\frac{1}{C_s}\left(\frac{g_m}{\omega^2 C_g}+\frac{C_g}{g_m}\right)+\frac{C_s}{C_g g_m}+\frac{2}{g_m}\geq 2\sqrt{\frac{1}{\omega^2 C_g^2}+\frac{1}{g_m^2}}+\frac{2}{g_m}. \quad [5]$$

Note that Eq. [5] defines the magnitude of negative resistance, which, according to Eq. [1] should be larger than the parallel resistance of the coil in order for the combined resistance to remain positive. As the optimization relation implies, C_g should be less than C_s and ωC_s should be less than g_m. Since the negative resistance is comparable to the parallel resistance of the coil, Eq. [4] indicates that the susceptance of C_g and C_s and the transconductance need to be reduced to a few mS for the circuit to remain stable. The 11 mm diameter coil L_0 has an inductance of 24 nH, and a parallel resistance of 2.0 kΩ based on the relation $R_{LC}=\omega L Q_{LC}$. To obtain a gain of four, we increase the apparent Q by a factor of four by reducing $|R_{neg}|$ to 2.67 kOhm. A bias current ~0.1 mA is required to reduce the transconductance to ~2 mS. The gate capacitance C_g was increased to 1.5 – 2.5 pF with an external capacitor. Using the minimization relation, $C_s^2 = C_g^2 + g_m^2/\omega^2$, a nominal value of 4 pF is estimated for C_s, which is provided by the varactor when reverse-biased at 2 Volts. The gain of the circuit is adjusted by voltage across C_s. The voltage on the drain is reduced to 0.8 Volts to minimize the dissipated power.

As Eq. [1] indicates, it is desirable to obtain larger Q_{eff} to maximize amplifier gain. However, as Q_{eff} increases, the bandwidth of the coil decreases, which is ultimately limited by the bandwidth required for imaging. For example, if 1 dB signal variation is allowed within the imaging bandwidth, the −3 dB bandwidth of the coil needs to be about twice this bandwidth. A 50 kHz imaging bandwidth translates to a minimum bandwidth of 100 kHz for the coil. For the Siemens 3T scanner with a center frequency of 123.24 MHz, the 100 kHz bandwidth sets an upper limit for Q_{eff} of about 1200. Since Q_{LC} for the 11 mm coil is about 105, maximum gain of the circuit using Q_{eff}/Q_{LC} is about 20 dB at this frequency.

The GaAs HEMT has substantial g_m even at low currents, which varies approximately as the square root of current (10). Even when biased at ~0.1 mA, the low noise property of HEMT is still maintained. The noise current from the drain-source channel decreases with decreasing drain current (11–13). The minimum noise figure, F_{min} (13–14), also decreases with drain current, but eventually begins to rise as g_m becomes too small and noise mismatch develops at the input of the transistor (11). This increase in noise figure was attributed to the resistive connections to the die in early transistors. However, fabrication techniques have improved, as evidenced by the reduction in device noise figures (13–15), and newer devices can operate at lower bias currents.

All MR experiments were performed on a Skyra 3T (Siemens AG, Erlangen, Germany) clinical scanner operating at 123.24 MHz. A Siemens 4-channel Flex Coil positioned horizontally and interfaced to the side of the patient table was used as an external receive coil. The phantoms were fabricated from 8 mm thick plastic weigh-boats filled with 1% agarose gel containing 0.9% NaCl to provide loading, and 1 mM Gadavist (Bayer, NJ) to yield a T_1 = 0.25 sec. To obtain baseline SNR from the gel, the Flex coil was replaced with a tuned and matched 11 mm coil connected directly to the Flex Coil interface. Next, a passive 11 mm coil of the same diameter was placed on the gel. The coil and gel were then positioned centrally above the #2 element of the Flex Coil in the magnet, so that the passive loop coupled MR signals from the gel to the Flex Coil. Images were acquired for several locations of the passive loop and gel above the Flex coil and SNR's evaluated.

The negative resistance detector was investigated similarly. The detector was first positioned on a gel and tuned on the bench using the trim capacitor C_t. The detector and gel were then imaged at the same four locations as for the passive loop and gel. The transistor of the amplifier was oriented parallel to the B_0 field to avoid noise degradation by Hall effect. The gain of the negative resistance detector was maximized empirically by adjusting the bias voltage V_2. SNR's from this setup were then compared with SNR's of the passive loop and with the surface coil that was connected directly to the Flex Coil interface.

Finally, the negative resistance detector was used to acquire images from the head of a 30 g mouse. The detector was first tuned on the head of the mouse before being moved to the scanner room for imaging. The Flex Coil was positioned above the animal and detector, the signal was optimized using the external voltage control, and the B_o field was shimmed over the head of the animal prior to acquiring images.

Results

Bench measurements were performed to evaluate detector performance under sample loading conditions. S_{21} was measured with a double pick-up loop connected to both ports of a network analyzer. When V_1 and V_2 were zero, a reference curve was obtained without gain. V_1 was then set to 0.8 V to power the transistor, and measurements were performed with a series of bias voltages V_2 applied to the source varactor C_s to maximize detector gain (Fig. 2a). The gain was determined by comparing the height of each curve with respect to the peak position of the reference curve. A maximum gain of 14 dB was reached when V_1 = 0.8 V and V_2 = 2 V. Concomitantly, the −3 dB bandwidth decreased to 240 kHz, providing an imaging bandwidth of about half this value. Fig. 2b shows the negative resistance estimated from Eq. [1] with R_{LC} computed from $R_{LC} = \omega L Q_{LC}$, where Q_{LC} is the Q measured from the reference curve. As the source capacitance varies, $|R_{neg}|$ reaches a minimum. By equating the last term of Eq [5] with the measured value of $|R_{neg}|$ (2.45 kΩ), and equating C_g = 2.2 pF, which includes 1.2 pF from the external chip capacitor, g_m is estimated to be 2.1 mS.

To demonstrate the sensitivity advantage for different coupling conditions, the passive coil and the active coil were tested at four locations along the axis of one element of the Flex Coil. Baseline SNR was first measured by a 11-cm diameter coil balance matched to a 50 Ohm cable that was connected to the same port as the #2 element of the Flex Coil. Coronal images were then acquired from passive and active detectors to measure SNR at four locations above the Flex coil. Typical coronal images are shown in Fig. 3a, and the relative SNR's from the passive coil and the active coil are shown in Fig. 3b.

At 3 cm separation from the external coil, the SNR of the coil with direct wire connection was 0.8 dB higher than that of the active detector and 5.6 dB higher than the passive detector. The latter reflects the transmission efficiency of inductive coupling, and the former reflects the combined effects of the negative resistance amplifier and the attenuation from inductive coupling. The trend in the plot along the direction of closer proximity suggests that the amplifier adds even less noise than this, perhaps on the order of 0.5 dB. For larger separations, attenuation dominates over the gain, and the curve for active coil becomes asymptotically parallel to that of the passive coil. The 11 dB difference reflects the amplifier gain inside the scanner. Higher gains are achievable; however, tuning of the active coils becomes more difficult for higher Q's.

To demonstrate biomedical applications of the detector, high resolution images were acquired from the head of a mouse (Fig. 4). The gain of the device was sufficient to obtain images with 156 × 156 μm^2 in-plane resolution and 0.3 mm slice thickness on the Siemens 3T clinical scanner, yielding SNR's of 48.6 for the coronal image and 50.3 for the saggital image. Anatomical details of mouse head are readily obtainable at this resolution. The filter bandwidth for imaging was 19.2 kHz, which was well within the tuning bandwidth of the detector. No modifications to the scanner interface were required.

Discussion

An MR detector with an integrated amplifier has been constructed that utilizes the positive feedback of a transistor to amplify the current in the sample coil. This feedback effect takes place as if the resonant sample coil were connected in parallel with a negative resistance, increasing the quality factor of the coil. This amplification can compensate for most of the sensitivity loss incurred when the NMR signal is inductively coupled to an external receive coil. A varactor connected between the transistor's source and ground allows the gain to be controlled dynamically. Since the integrated detector has very high Q, a trade-off exists between the gain and the bandwidth. Here, a detector with an 11-mm diameter loop yielded 14-dB of gain and a 3-dB bandwidth of 240 kHz. By inductively coupling the remote detector to the commercial coil, no additional interface to the system was required. When the remote detector was used in close proximity to the commercial coil, the sensitivity of the detector was comparable to that of a direct-wire connection. To obtain a larger FOV, amplifiers could be placed on two or more coils of an array, but this would require that they be geometrically or capacitively decoupled from one another with care (16,17). Any residual inductive coupling will be magnified by the increased Q's of each circuit. The capability of the detector was demonstrated with high resolution animal imaging on a clinical scanner. This bodes well for other clinical applications involving imaging of superficial and internal tissues. Efficient signal transmission via on-coil amplification should make it easier to interface custom designed detectors with standard clinical coils.

There are several advantages for using local amplification of the MR signal. First, it provides an *in situ* amplifier that can be attached to the LC resonator without the need for impedance matching. Second, the negative resistance amplifier can operate at very low bias current without sacrificing noise performance. This is mainly because channel noise associated with the drain current falls as the bias current is reduced (18). At lower bias currents, noise from the gate becomes comparable to thermal noise in the channel, but this does not happen for bias currents used here. The negative resistance amplifier tested here consumed only 88 μW of power. With such low power consumption, an amplifier for an implantable device may benefit from wireless power harvesting schemes (19). For external applications, the negative resistance amplifier can be powered with batteries and used with commercially available coils of much larger dimensions without the need to interface it to the scanner. Finally, since negative resistance amplification provides a method for artificially manipulating the Q of a sample circuit, especially in coils with homogenous field, one could potentially use them for novel nonlinear experiments involving radiation damping (20,21), which has been used to improve contrast in MRI (22).

Acknowledgement

Helpful discussions with Dr. Grieg Scott are gratefully acknowledged. This research was supported by the Intramural Research Program of the NINDS at NIH and R00EB016753.

References

1. Wheeler D, Conradi M. Practical exercises for learning to construct NMR/MRI probe circuits. Concepts in Magnetic Resonance A. 2012; 40A(1):1–13.

2. Schnall MD, Barlow C, Subramanian VH, Leigh JS. Wireless Implanted Magnetic-Resonance Probes for in vivo NMR. J Magn Reson. 1986; 68(1):161–167.
3. Olson DL, Peck TL, Webb AG, Magin RL, Sweedler JV. High-Resolution Microcoil H-1-NMR for Mass-Limited, Nanoliter-Volume Samples. Science. 1995; 270(5244):1967–1970.
4. Qian CQ, Murphy-Boesch J, Dodd S, Koretsky A. Sensitivity enhancement of remotely coupled NMR detectors using wirelessly powered parametric amplification. Magn Res Med. 2012; 68(3): 989–996.
5. Qian CQ, Yu X, Chen DY, Dodd S, Bouraoud N, Pothayee N, Chen Y, Beeman S, Bennett K, Murphy-Boesch J, Koretsky A. Wireless Amplified Nuclear MR Detector (WAND) for High-Spatial-Resolution MR Imaging of Internal Organs: Preclinical Demonstration in a Rodent Model. Radiology. 2013; 268(1):228–236. [PubMed: 23392428]
6. Collin, RE. Foundations for Microwave Engineering. NY: McGraw-Hill; 1966.
7. Syms RRA, Solymar L, Young IR. Three-frequency parametric amplification in magneto-inductive ring resonators. Metamaterials. 2008; 2:122–134.
8. Qian C, Zabow G, Koretsky A. Engineering novel detectors and sensors for MRI. J. Magn Reson. 2013; 229:67–74. [PubMed: 23245489]
9. Lee, T. Planar Microwave Engineering: A Practical Guie to Theory, Measurement, and Circuits. London: Cambridge University Press; 2004. p. 420-427.
10. Ellinger, F. Radio Frequency Integrated Circuits and Technologies. Berlin: Springer-Verlag; 2008. p. 516
11. Statz H, Haus H, Pucel R. Noise Characteristics of Gallium Arsenide Field-Effect Transistors. IEEE Trans on Electron Devices. 1974; ED21(9):549–562.
12. Pucel, R.; Haus, H.; Statz, H. Signal and Noise Properties of GaAs Microwave FET. NY: Academic Press; 1975. p. 195-265.
13. Van der Ziel, A. Noise and Solid State Devices and Circuits. NY: John Wiley & Sons; 1986. p. 306
14. Technical Data Sheet for ATF-34143 GaAs Transistor: Agilent Technologies. 2001
15. Pospieszalski MW. Modeling of noise parameters of MESFETs and MODFETs and their frequency and temperature dependence. IEEE Trans Microwave Theory Tech. 1989; MTT-37(9): 1340–1350.
16. Zhang XZ, Webb A. Design of a capacitively decoupled transmit/receive NMR phased array for high field microscopy at 14.1 T. J. Magn Reson. 2004; 170(1):149–155. [PubMed: 15324768]
17. Lee RF, Giaquinto RO, Hardy CJ. Coupling and decoupling theory and its application to the MRI phased array. Magn Reson Med. 2002; 48(1):203–213. [PubMed: 12111947]
18. Ambrozy, A. Electronic Noise. NY: McGraw-Hill Internationl Books; 1982.
19. Riffe MJ, Heilman JA, Griswold MA. Power scavenging circuit for wireless DC power. Proc Int Soc Magn Reson Med. 2007:3273.
20. Louis-Joseph A, Lallemand JY, Abergel D. Nonlinear dynamics of a magnetization subject to RF feedback field: new experimental evidence. Comptes Rendus Chimie. 2004; 7(3–4):329–333.
21. Huang SY, Lin YY, Lisitza N, Warren WS. Signal interferences from turbulent spin dynamics in solution nuclear magnetic resonance spectroscopy. J. Chem Phys. 2002; 116(23):10325–10337.
22. Huang SY, Wolahan SM, Mathern GW, Chute DJ, Akhtari M, Nguyen ST, Huynh MN, Salamon N, Lin YY. Improving MRI differentiation of gray and white matter in epileptogenic lesions based on nonlinear feedback. Magn Reson Med. 2006; 56(4):776–786. [PubMed: 16941616]

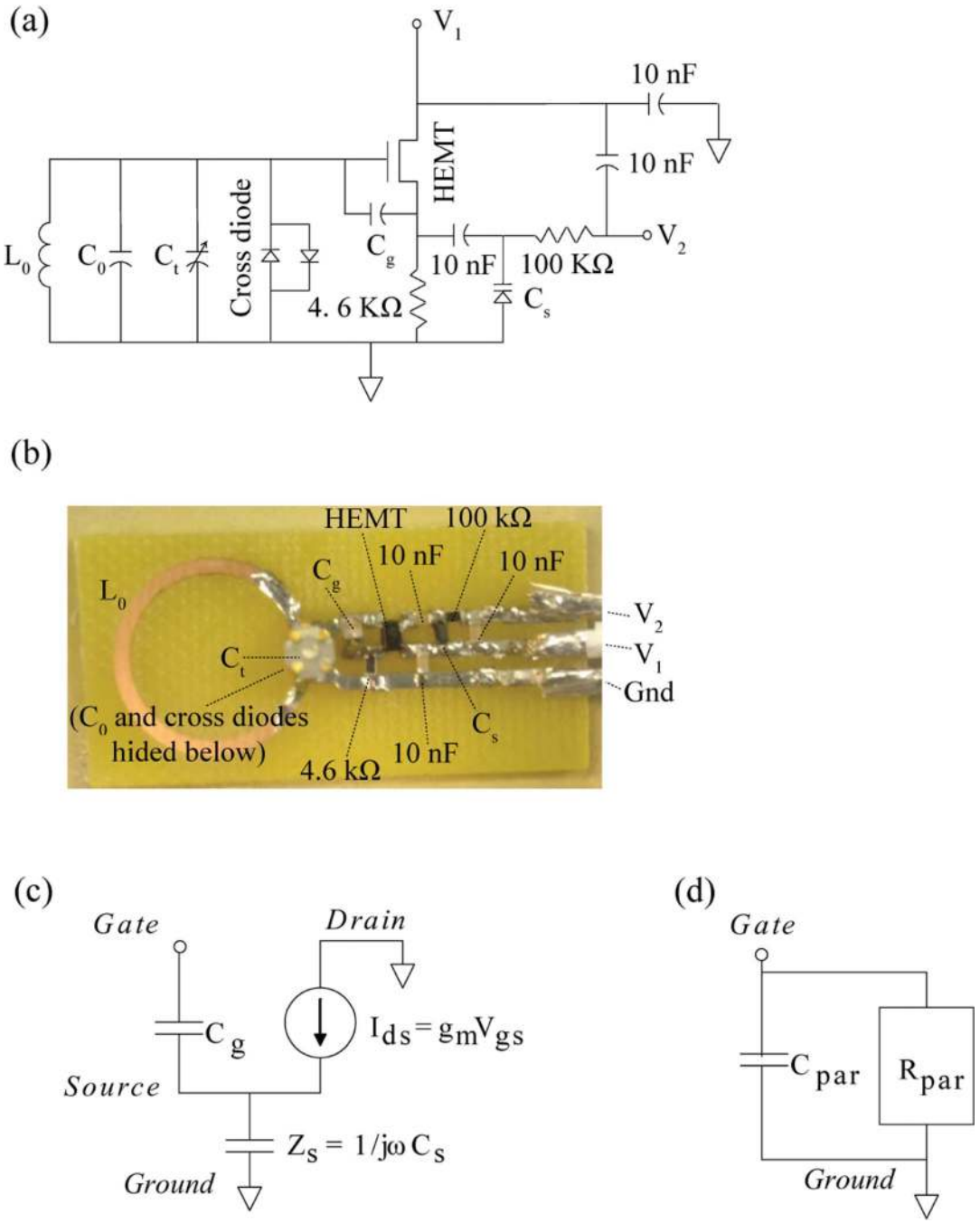

Fig. 1.

The schematic (a) and a photograph (b) of the negative resistance circuit. A low-frequency model of transistor and circuit in grounded drain configuration is shown in (c). In (d) the admittance Y_g at the gate terminals can be represented as a gate capacitance in parallel with a (lossless) negative resistance.

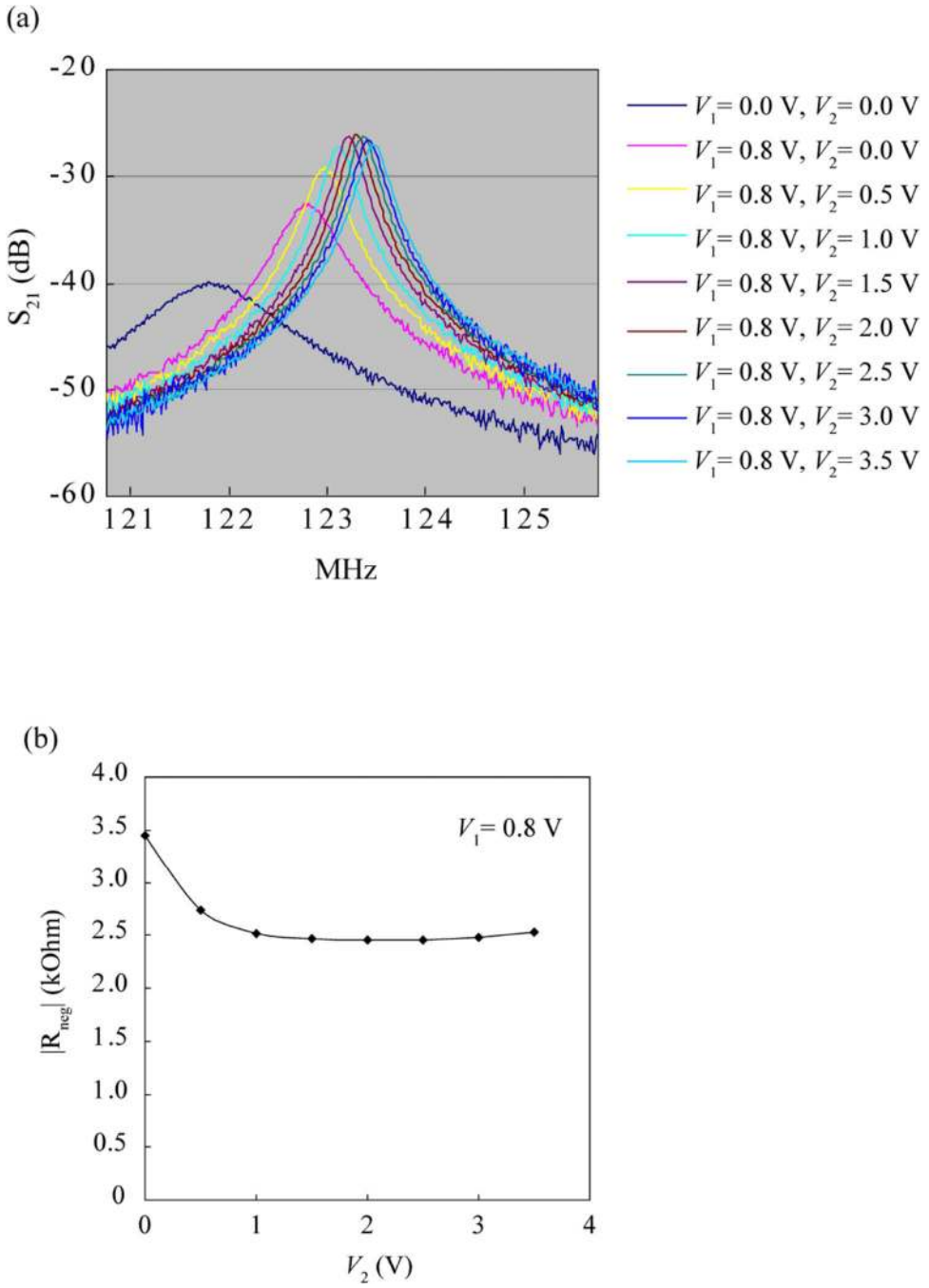

Fig. 2.

(a) S_{21} transmission curves measured with a double pick-up loop positioned above the sample coil and connected to an Agilent E5061A network analyzer. The left most curve was measured without any bias voltage applied to the source varactor C_s. With the drain of the transistor biased at 0.8 V, a series of curves were measured with the source varactor biased from 0 V to 3.5 V in 0.5 V steps, respectively. (b) For each biasing condition, $|R_{neg}|$ was evaluated from Eq. [1], as described in the text, with the optimum value occurring at 2 V.

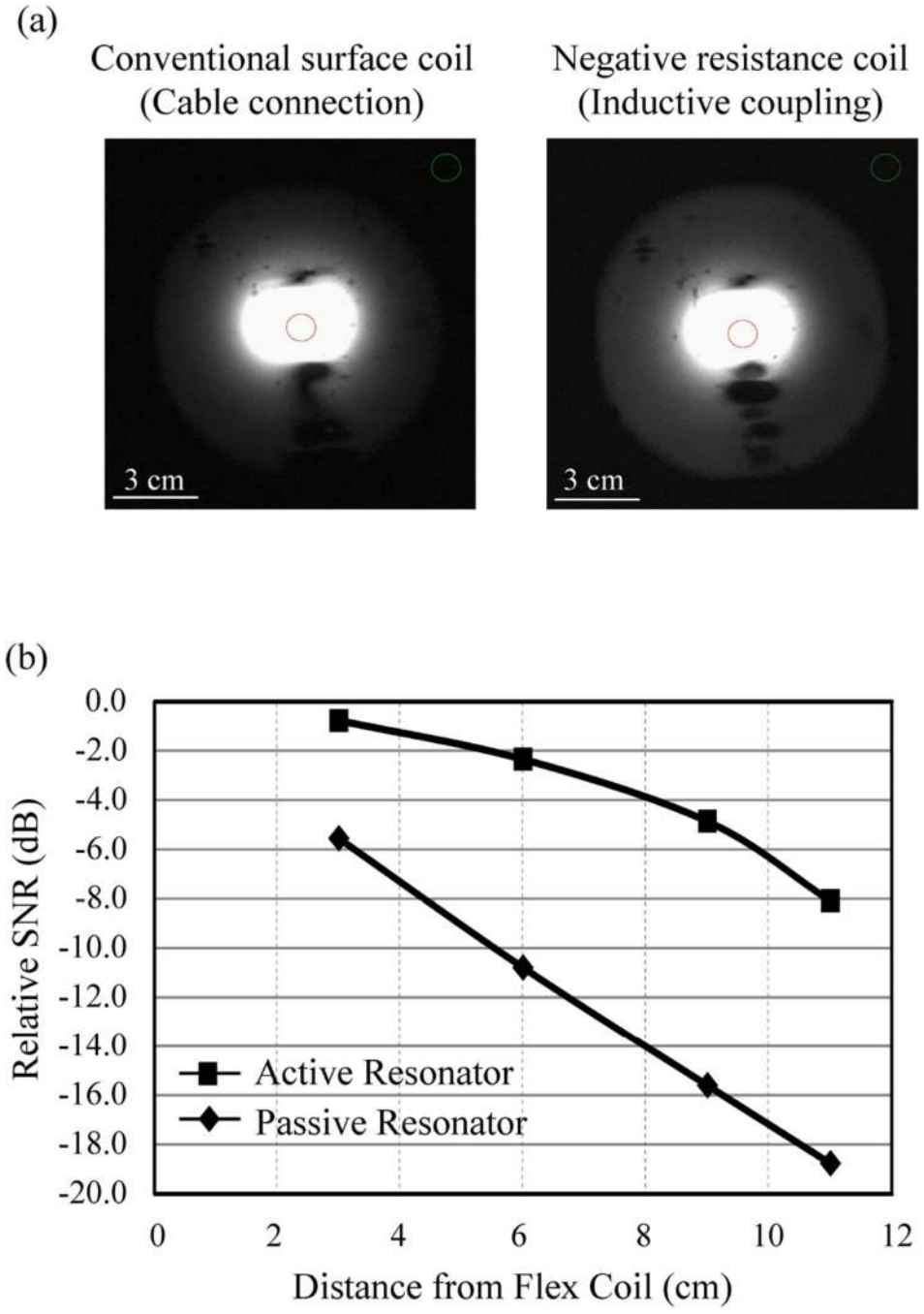

Fig. 3.

(a) Zoomed in view of coronal images of the gel samples with a scaling factor of 2. The sample was first scanned with a coil with direct wire connection to the scanner receiver, and then with the negative resistance resonator placed in close proximity (3 cm) to the #2 element of the Siemens Flex coil. The SNR was evaluated in the regions defined by the small circles. (b) SNR data obtained from the coronal images normalized to the single SNR obtained from the coil with direct cable connection to the scanner interface. SNR's were obtained from a passive coil and gel placed at four locations along the axis of the #2 element

of the Flex coil (nominal radius = 6.5 cm), and from the active coil and sample from the same locations. Acquisition parameters for all SNR measurements were: TE = 5.4 ms, TR = 500 ms, FA = 90 deg, NS = 1, in-plane resolution 252 × 252 μm^2, FOV = 12.9 × 12.9 cm^2, slice thickness = 1.5 mm.

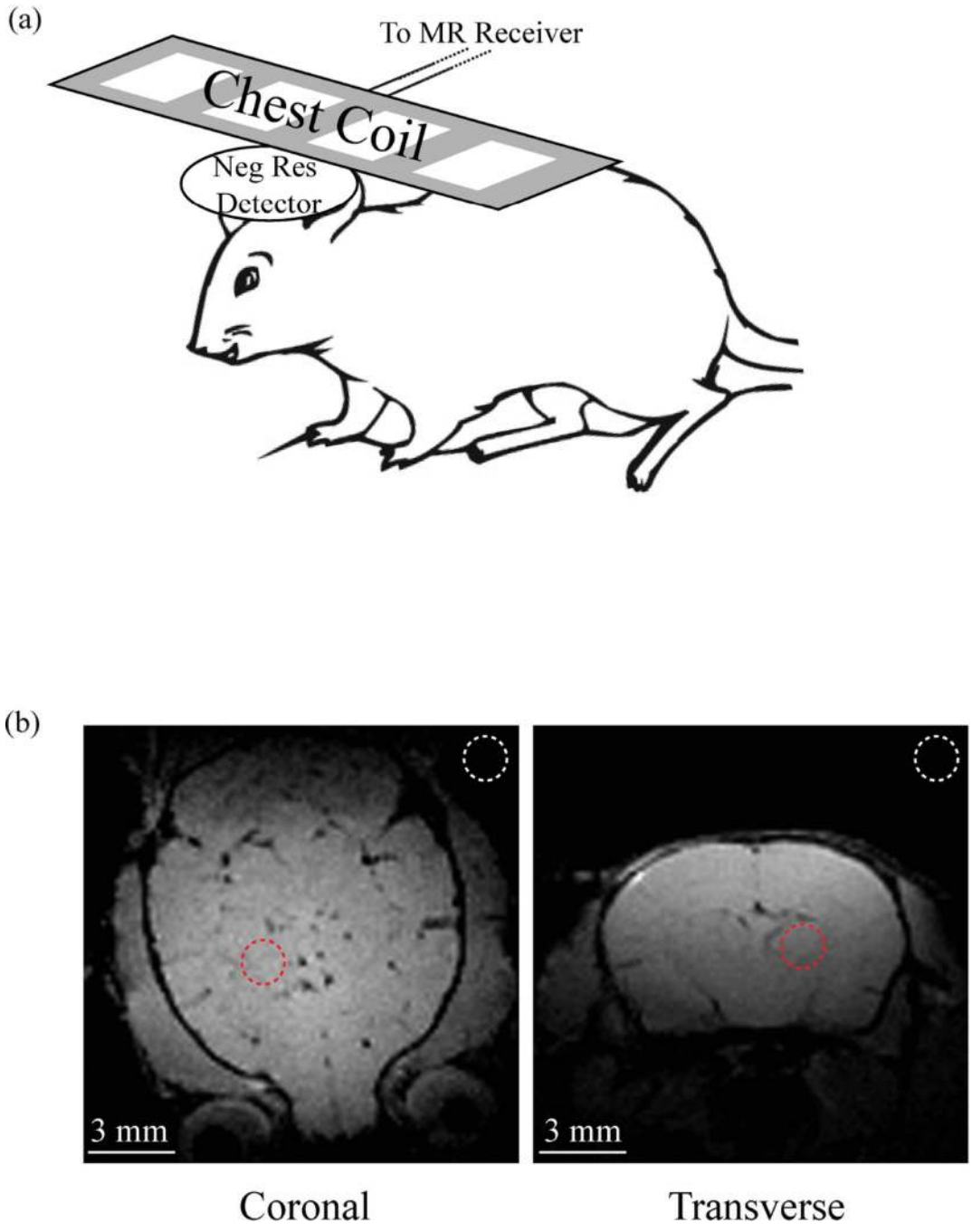

Fig. 4.

(a) A schematic illustration of a negative resistance detector placed on mouse head to enhance local detection sensitivity. The negative resistance detector is inductively coupled to a much larger chest coil used in a clinical MRI scanner. (b) The coronal and transverse images from the head of a mouse acquired on the Skyra 3T Siemens scanner. Both images have an in-plane resolution of 156 × 156 μm^2 and slice thickness of 0.3 mm. Images were acquired with FOV = 3 × 3 cm^2, TE = 12.9 ms, TR = 575 ms, FA = 40 deg, NS = 4, and an

imaging bandwidth of 19.2 kHz. The SNR was evaluated in the regions defined by the small circles.